# Chemoselective imaging of mouse brain tissue via multiplex CARS microscopy

**Christoph Pohling,[1] Tiago Buckup,[1] Axel Pagenstecher,[2] and Marcus Motzkus[1,*]**

[1]*Physikalisch-Chemisches Institut, Ruprecht-Karls-Universität, Im Neuenheimer Feld 229, D-69120 Heidelberg, Germany*

[2]*Abteilung Neuropathologie, Universität Marburg, Baldingerstr.1, D-35043 Marburg, Germany*

**marcus.motzkus@pci.uni-heidelberg.de*

**Abstract:** The fast and reliable characterization of pathological tissue is a debated topic in the application of vibrational spectroscopy in medicine. In the present work we apply multiplex coherent anti-Stokes Raman scattering (MCARS) to the investigation of fresh mouse brain tissue. The combination of imaginary part extraction followed by principal component analysis led to color contrast between grey and white matter as well as layers of granule and Purkinje cells. Additional quantitative information was obtained by using a decomposition algorithm. The results perfectly agree with HE stained references slides prepared separately making multiplex CARS an ideal approach for chemoselective imaging.



**OCIS codes:** (180.0180) Microscopy; (170.0170) Medical optics and biotechnology; (300.6230) Spectroscopy, coherent anti-Stokes Raman scattering

## References and links

1. A. Zumbusch, G. R. Holtom, and X. S. Xie, "Three-dimensional vibrational imaging by coherent anti-Stokes Raman scattering," Phys. Rev. Lett. **82**(20), 4142–4145 (1999).
2. A. Volkmer, J. X. Cheng, L. D. Book, and X. S. Xie, "New advances in Coherent anti-Stokes Raman scattering (CARS) microscopy and spectroscopy of biological systems," Biophys. J. **80**, 164a (2001).
3. M. Harz, P. Rösch, and J. Popp, "Vibrational spectroscopy--a powerful tool for the rapid identification of microbial cells at the single-cell level," Cytometry A **75A**(2), 104–113 (2009).
4. H. W. Wang, T. T. Le, and J. X. Cheng, "Label-free imaging of arterial cells and extracellular matrix using a multimodal CARS microscope," Opt. Commun. **281**(7), 1813–1822 (2008).
5. M. Okuno, H. Kano, P. Leproux, V. Couderc, and H. O. Hamaguchi, "Ultrabroadband multiplex CARS microspectroscopy and imaging using a subnanosecond supercontinuum light source in the deep near infrared," Opt. Lett. **33**(9), 923–925 (2008).
6. A. Dogariu, A. Goltsov, and M. O. Scully, "Real-time monitoring of blood using coherent anti-Stokes Raman spectroscopy," J. Biomed. Opt. **13**(5), 054004 (2008).
7. H. A. Rinia, M. Bonn, E. M. Vartiainen, C. B. Schaffer, and M. Müller, "Spectroscopic analysis of the oxygenation state of hemoglobin using coherent anti-Stokes Raman scattering," J. Biomed. Opt. **11**(5), 050502 (2006).
8. C. L. Evans, X. Y. Xu, S. Kesari, X. S. Xie, S. T. C. Wong, and G. S. Young, "Chemically-selective imaging of brain structures with CARS microscopy," Opt. Express **15**(19), 12076–12087 (2007).
9. C. L. Evans and X. S. Xie, "Coherent anti-stokes Raman scattering microscopy: chemical imaging for biology and medicine," Annu Rev Anal Chem (Palo Alto Calif) **1**(1), 883–909 (2008).
10. C. Krafft, B. Dietzek, and J. Popp, "Raman and CARS microspectroscopy of cells and tissues," Analyst (Lond.) **134**(6), 1046–1057 (2009).
11. C. Krafft, L. Shapoval, S. B. Sobottka, K. D. Geiger, G. Schackert, and R. Salzer, "Identification of primary tumors of brain metastases by SIMCA classification of IR spectroscopic images," Biochim. Biophys. Acta **1758**(7), 883–891 (2006).
12. C. Krafft, G. Steiner, C. Beleites, and R. Salzer, "Disease recognition by infrared and Raman spectroscopy," J Biophotonics **2**(1-2), 13–28 (2009).
13. B. Bird, M. Miljković, N. Laver, and M. Diem, "Spectral detection of micro-metastases and individual metastatic cells in lymph node histology," Technol. Cancer Res. Treat. **10**(2), 135–144 (2011).
14. E. M. Vartiainen, "Phase Retrieval Approach for Coherent Anti-Stokes-Raman Scattering Spectrum Analysis," J. Opt. Soc. Am. B **9**(8), 1209–1214 (1992).
15. H. A. Rinia, M. Bonn, M. Müller, and E. M. Vartiainen, "Quantitative CARS spectroscopy using the maximum entropy method: the main lipid phase transition," ChemPhysChem **8**(2), 279–287 (2007).
16. Y. X. Liu, Y. J. Lee, and M. T. Cicerone, "Fast extraction of resonant vibrational response from CARS spectra with arbitrary nonresonant background," J. Raman Spectrosc. **40**(7), 726–731 (2009).

#147302 - $15.00 USD Received 11 May 2011; revised 27 Jun 2011; accepted 27 Jun 2011; published 30 Jun 2011

17. C. Krafft, A. A. Ramoji, C. Bielecki, N. Vogler, T. Meyer, D. Akimov, P. Rösch, M. Schmitt, B. Dietzek, I. Petersen, A. Stallmach, and J. Popp, "A comparative Raman and CARS imaging study of colon tissue," J Biophotonics **2**(5), 303–312 (2009).
18. T. Meyer, N. Bergner, C. Bielecki, C. Krafft, D. Akimov, B. F. M. Romeike, R. Reichart, R. Kalff, B. Dietzek, and J. Popp, "Nonlinear microscopy, infrared, and Raman microspectroscopy for brain tumor analysis," J. Biomed. Opt. **16**(2), 021113 (2011).
19. B. von Vacano, L. Meyer, and M. Motzkus, "Rapid polymer blend imaging with quantitative broadband multiplex CARS microscopy," J. Raman Spectrosc. **38**(7), 916–926 (2007).
20. C. Pohling, T. Buckup, and M. Motzkus, "Hyperspectral data processing for chemoselective multiplex coherent anti-Stokes Raman scattering microscopy of unknown samples," J. Biomed. Opt. **16**(2), 021105 (2011).
21. T. W. Kee and M. T. Cicerone, "Simple approach to one-laser, broadband coherent anti-Stokes Raman scattering microscopy," Opt. Lett. **29**(23), 2701–2703 (2004).
22. H. Kano and H. Hamaguchi, "Dispersion-compensated supercontinuum generation for ultrabroadband multiplex coherent anti-Stokes Raman scattering spectroscopy," J. Raman Spectrosc. **37**(1-3), 411–415 (2006).
23. E. M. Vartiainen, H. A. Rinia, M. Müller, and M. Bonn, "Direct extraction of Raman line-shapes from congested CARS spectra," Opt. Express **14**(8), 3622–3630 (2006).
24. R. Viviani, G. Grön, and M. Spitzer, "Functional principal component analysis of fMRI data," Hum. Brain Mapp. **24**(2), 109–129 (2005).
25. A. Mizuno, T. Hayashi, K. Tashibu, S. Maraishi, K. Kawauchi, and Y. Ozaki, "Near-infrared FT-Raman spectra of the rat brain tissues," Neurosci. Lett. **141**(1), 47–52 (1992).
26. K. V. Branden and M. Hubert, "Robust classification in high dimensions based on the SIMCA method," Chemom. Intell. Lab. Syst. **79**(1-2), 10–21 (2005).

## 1. Introduction

Coherent anti-Stokes Raman scattering (CARS) is a widespread technique in nonlinear microscopy of biological structures [1,2]. CARS has been applied in a large field of medical applications ranging from the identification of microbial cells, high resolution imaging of human aorta-tissue, time resolved observations of HELA cells, up to real time monitoring of blood oxygenation level [3–7]. In spite of its success, CARS has been used only rarely for the identification of pathologic tissue alterations [8–10]. This contrasts to linear techniques like Raman and infrared spectroscopy, which were already successfully correlated with histological characterization and classification of cancer types in human brain and lymph tissue [11–13].

The main challenge of the use of CARS in such applications is mainly due to two reasons. First, as a coherent process, CARS spectra show interference effects between the Raman resonances and the so called nonresonant background that introduces dispersive line profiles finally responsible for the distortions of line shape. Such distortions of spectral lines lead to loss of spectral information, especially for weak Raman modes in the presence of strong resonances and noise. Phase retrieval algorithms were already discussed to circumvent such problems [14–16], but have not been applied regularly. The second issue is the spectral resolution, which is often limited by ultrashort laser pulses necessary to stimulate the nonlinear effects. CARS studies of brain tissue discussed so far circumvented the disadvantage of low spectral resolution by using a synchronized pair of ps-laser sources with a frequency difference matching a single vibrational mode of the sample [8]. In this case, the image contrast is based mostly at the intense CH-stretching vibrational mode of lipids around 2900 $cm^{-1}$. As a consequence, CARS investigation of brain tissue could not take advantage of modern multivariate data analysis [17] as it is performed with spontaneous Raman spectroscopy [18]. Recently we have addressed thoroughly these two challenges in CARS microscopy by combining multiplex CARS (MCARS) [19] with a "two-step" analysis procedure [20]. In this regard, we have extracted the Raman information from the MCARS raw data and classified it afterwards by multivariate statistics. This procedure led to a chemoselective image of complex structured polymer samples and biological samples. Here, we exploit the "two-step" method and apply it to MCARS studies of mouse brain tissue in order to obtain chemoselective image contrast based on a full Raman spectrum. The results were compared to brightfield images of hematoxylin and eosin (H&E) stained references and to lipid intensity contrasted images of MCARS raw data.

#147302 - $15.00 USD Received 11 May 2011; revised 27 Jun 2011; accepted 27 Jun 2011; published 30 Jun 2011

## 2. Experimental section

The MCARS experimental setup is illustrated in Fig. 1. The most important issues have been already described [19–22]. It is based on the 1.0 W output power of a Ti:sapphire fs-oscillator (Coherent Mira), with the 6 nm-wide spectrum (FWHM) that is split in two parts. About 100 mW are reflected into an end sealed photonic crystal fiber (crystal fiber, A/S) whereas the second part passes a narrowband filter of 1 nm FWHM. The resulting broadband continuum as well as the narrowband pulse is coupled into a commercially available light microscope modified for MCARS imaging. The setup has been equipped with a 50x IR corrected microscope objective with high working distance (Olympus LMPlan50xIR) and piezo driven sample holder. The signal ranging from 500 to 3400 $cm^{-1}$ is detected by a CCD camera (Andor Idus). A sample area of 100x100 µm was raster scanned with a step size of 1 µm for each scan. The acquisition time per pixel was 200 ms. After submission of this work, we improved our setup regarding hardware and software, which allows measurements as fast as 4 minutes, with pixel dwell times of 20 ms without lowering the signal to noise ratio. Total average power in the focus volume was less than 30 mW.

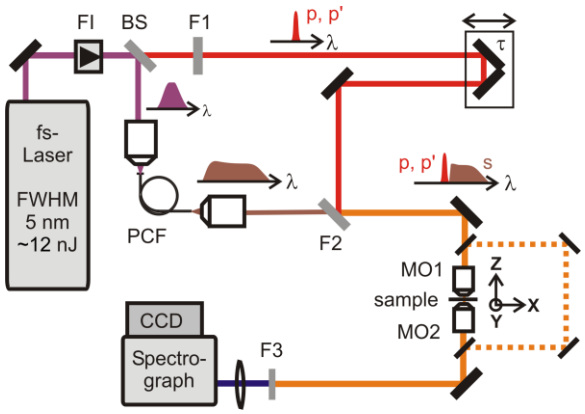


Fig. 1. MCARS experimental setup. BS, beam splitter; F1, band pass filter cuts out the narrowband pump and probe beam; PCF, photonic crystal fiber broadens the Stokes beam; F2, long pass filter where pump and Stokes are spatially overlaid again; MO1, microscope objective for measurement; MO2, microscope objective for signal output collimation; F3, short pass filter.

The procedure of image processing consists of two separate steps described in detail in ref [20]. Here, we briefly review the most important aspects. Firstly, the extraction of the Raman information is performed: In our previous investigation we applied a recently developed FFT based fitting algorithm [16]. In the present work we expand our repertoire and demonstrate the combination of the well-known maximum entropy method (MEM) [14,23] with our two-step approach. The MEM-approximation is applied directly to the CARS raw data and does not require background subtraction. This can be an important advantage of MEM-approximation over other methods for systems where it is difficult to estimate the non-resonant background. As second step, principal component analysis (PCA) classified the spectra in terms of orthonormal weight vectors that highlight differences and patterns within the data set. The three highest valued weight vectors were taken as a new orthonormal base for the measured data. The projection of every spectrum in the new basis was designated to the colors green, red and blue in order to establish a RGB-false color image of the sample, the so called score plot [24]. The data post processing takes currently about 20 minutes for Raman extraction and about 2 minutes for PCA calculation in case of 10.000 MCARS spectra with 428 data points each. It was carried out on a standard personal computer with Pentium dual core 2,2 GHz processor and 2 GB RAM. MEM and the eigenanalysis task itself are not supervised and can be used as an automatic procedure.

#147302 - $15.00 USD Received 11 May 2011; revised 27 Jun 2011; accepted 27 Jun 2011; published 30 Jun 2011

Concerning the application to biological samples, sections (20 µm) of fresh mouse brain tissue were prepared. Every other slide was stained with hematoxylin-eosin (H&E) as a reference that allowed for the microscopic identification of the different cells. The native slides, all transparent in bright field contrast, were taken for the CARS experiments and air tightly sealed (Gene-Frame, Thermo Scientific, UK) in order to prevent desiccation. No additional water was added to avoid moisture expansion.

## 3. Results and Discussion

In Fig. 2 we compare the bright field contrasted images of the HE stained slides with our results of MCARS experiment. Figure 2(a) shows a portion of the cerebellar white matter (asterisks) bordered by the granule cell layers (lower left and upper right, blue staining reflects the nuclei of the granule cells). Figure 2(b) shows the regular cerebellar architecture: myelin on top followed by the granule cell layer which is followed by the Purkinje-cell layer (arrows) and the molecular cell layer. In order to evaluate MCARS analyzed by our two-step method, we selected different areas of the HE stained slides in Figs. 2(a) and (b). These areas are marked as black insets in Figs. 2(a) and (b) and the processed MCARS images are shown in Figs. 2(c) and (d), respectively. In Fig. 2(c) the lipid rich myelin provides the strongest signal and appears in green color. The granule cells expressed as scores of the second weight vector are shown in Red. The scores of the third vector are plotted in blue color enhancing the contrast between myelin and the granule cells. The MCARS based image in Fig. 2(d) allows also to differentiate between the granule cells (red), surrounding tissue (green) and the single layer of Purkinje cells that appear in purple as a mixing term of blue and red. Please note that the eigenvectors obtained by PCA cannot be directly compared between different data sets. As mentioned above, the MCARS data was collected from unstained slides that contain tissue which might be up to 20 µm separated from the associated reference. It follows that single nuclei of the granule cells appear at different positions than in Fig. 2(b). In the third column of

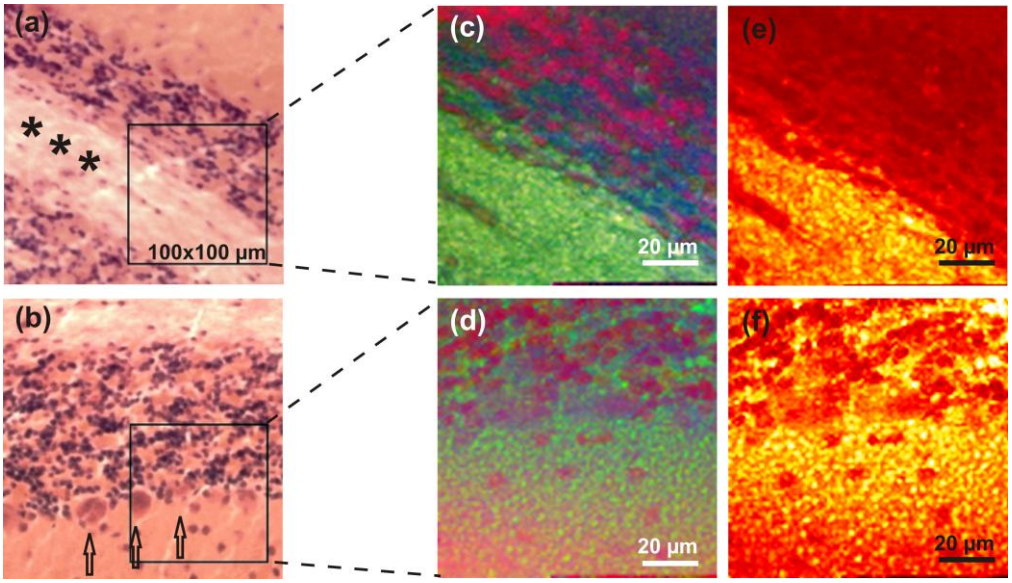


Fig. 2. Comparison of images taken by traditional bright field contrast of HE stained samples with our two step approach as well as the plot of the intensity at 2845 $cm^{-1}$ wavenumbers. (a) (b) Bright field image of three different slides stained by HE showing grey matter (orange), Purkinje cells (red), nuclei of granule cells (dark blue) and white matter (myelin, pink fiber bundles). (c), (d) The corresponding images of the boxed areas using MCARS microscopy, imaginary part extraction and PCA. White matter or myelin (bright green), nuclei of granule cells (red), Purkinje cells (purple) and grey matter (dark green) are reproduced accordingly. (e), (f) Contrast based on CH-vibrational mode of lipids, taken from the raw spectra at 2845 $cm^{-1}$.

#147302 - $15.00 USD Received 11 May 2011; revised 27 Jun 2011; accepted 27 Jun 2011; published 30 Jun 2011

Fig. 2, our method is compared to the contrast mechanism typically used in CARS microscopy with narrowband lasers, where the detection is constrained to single spectral features [9]. In this case, the intense CH-stretching vibrational mode taken from CARS raw data at 2845 $cm^{-1}$ provides image contrast when the signal strength is color coded from red to white. This method is mainly sensitive to dense and lipid rich sample components such as myelin appearing in bright structures in Figs. 2(e) and (f). On one hand, the color levels provide a well contrasted map of lipid intensities. On the other hand, different colors are not assigned to different spectral information and therefore lack an essential feature for tissue classification. This can be clearly seen, for example, in Figs. 2(c) and (e): In Fig. 2(c), granule cells (red) can be easily differentiated from myelin rich tissue (green), while Fig. 2(e) provides no further chemical information besides lipid contrast.

The false color mapping of Figs. 2(c) and (d) automatically provides biological image contrast and shows good agreement to the reference samples (Figs. 2(a) and (b)). However, this type of visualization is not quantitative hence the eigenvectors obtained in the PCA might not be considered as pure spectra. In previous works, we applied an evolutionary fitting procedure to the MCARS raw data in order to decompose quantitatively the composed spectra in its different components [19]. Unfortunately, the knowledge of the complex pure spectra was a prerequisite to decompose the data. Nevertheless, it is now possible to overcome this limitation when we extend our method: Fig. 3(a) shows the H&E stained reference of a tissue section with components similar to the samples presented in Fig. 2. Based on the corresponding CARS image result of the two-step method shown in Fig. 3(b) we can select the "pure spectra" at the marked positions of Fig. 3(b) for myelin (rectangle), neuropil (circle), granule cells (triangle) and a single Purkinje cell (inverted triangle). The quantitative information finally provided by the evolutionary fitting procedure is shown in Fig. 3 for myelin (Fig. 3(c)), grey matter (Fig. 3(d)), granule cells (Fig. 3(e)) and Purkinje cells (Fig. 3(f)), respectively. The fitting results provide complementary image information for all of the four components. The distribution of the different tissues matches with the result of Fig. 3(b) and both results are finally confirmed by the reference slide shown in Fig. 3(a). The component of Fig. 3(d) shows a homogeneous distribution over the sample area that also agrees to the presence of grey matter components, the neuropil, consisting of dendrites and axons, respectively. With respect to Figs. 3 (e) and (f) it is also possible to distinguish between two types of neuronal cells. The raw spectra (upper line, black-dotted), their MEM-approximation (upper line red-solid) as well as the extracted imaginary parts (lower lines) are shown in Figs. 3(g)-(j). The extracted Raman spectra show strong signal intensities between 2800 and 3000 $cm^{-1}$. This spectral region is assigned to the CH stretching vibrational modes namely at 2852 $cm^{-1}$ ($CH_2$ symmetric), 2885 $cm^{-1}$ ($CH_2$ asymmetric), 2938 $cm^{-1}$ ($CH_3$ symmetric) and 2958 $cm^{-1}$ ($CH_3$ asymmetric) [25]. Mizuno et al. also identified the spectral positions of 1442 $cm^{-1}$ and 1664 $cm^{-1}$ in rat brain tissue as the Raman-vibrational modes of amid (from proteins) and $CH_2$ deformation originating from lipid and proteins as well. Signals around 1480 $cm^{-1}$ and 1690 $cm^{-1}$ are also present in our extracted Raman information of Figs. 3 (g)-(j) and can be similarly explained. Additional weak signals can be estimated in the fingerprint region, e.g., around 1120 and 1320 $cm^{-1}$ in Fig. 3 (i), which are still lacking an assignment.

The quantitative distribution of different lipid components is a point of interest when CARS is applied in medical diagnostics. Hence, it can help to identify tumor margins that do not appear in bright field contrasted images. As an example of such an application, in Fig. 4 we compared three types of data analysis for monitoring the lipid distribution from the lower right to the upper left in Fig. 3 (along the diagonal dashed line in (b) and (c)). The simplest and mostly used approach is to plot the CH-stretching vibrational mode's intensity taken from the raw data at 2845 $cm^{-1}$. The variation of the intensity of this mode shows initially a steep decrease down to a level of about 40% of Myelin. The similar trend is well reproduced by taking the amplitude of the extracted linear Raman data set at 2860 $cm^{-1}$, which corresponds

#147302 - $15.00 USD Received 11 May 2011; revised 27 Jun 2011; accepted 27 Jun 2011; published 30 Jun 2011

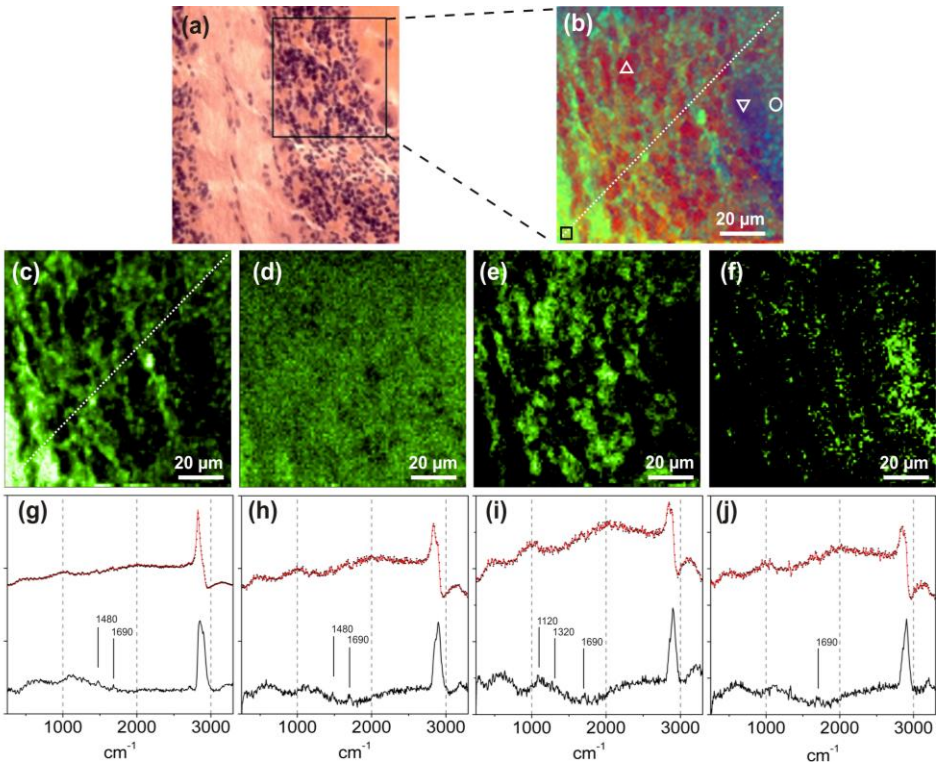


Fig. 3. Quantitative backward calculation of the sample components via evolutionary fitting based on the result obtained from the two step approach. (a) HE stained reference sample. (b) False color map using imaginary part extraction followed by PCA. (c)-(f) Quantitative fitting results of myelin, grey matter, granule cells and Purkinje cells, based on spectra selected at the white marked sample positions in b). (g)-(j) Corresponding spectral raw data (upper lines dotted) with MEM-approximation (solid line) as well as extracted imaginary parts (lower lines) taken at the selected sample positions.

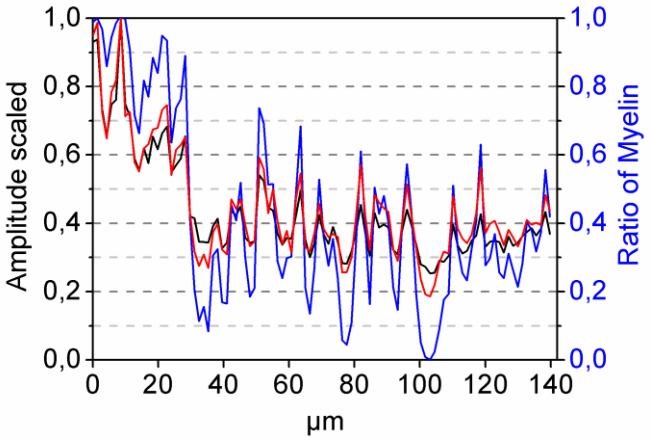


Fig. 4. Three different types of lipid monitoring along the diagonal line in Figs. 3(b) and (c). Red line: Extracted Raman intensity at 2860 $cm^{-1}$. Black line: Raw data intensity at 2845 $cm^{-1}$. Blue line: Quantitative fitting result according to Fig. 3(c) showing improved contrast and also a Myelin ratio which is not affected by other sample components anymore (zero amplitude).

#147302 - $15.00 USD Received 11 May 2011; revised 27 Jun 2011; accepted 27 Jun 2011; published 30 Jun 2011

to the blue shifted signal at 2845 $cm^{-1}$ in the MCARS raw data. Both methods, however, do not take into account the spectral overlapping of other contributions at the same spectral region and, therefore, cannot represent Myelin concentration exclusively. In contrast to that, by applying the two-step method followed by the evolutionary fitting algorithm, we are able to demonstrate that the real Myelin concentration shows a similar trend along the diagonal of Fig. 3(c), but with much higher accuracy and, in particular it also shows sample regions where Myelin is not present at all. The zero amplitude demonstrates that the Myelin ratio is not affected by other sample components anymore.

## 4. Conclusion and outlook

In conclusion, we have successfully obtained a chemo-selective image of brain tissue using MCARS. We have shown that our "two-step" method is able to provide chemical information even on biological tissues with high similarity and that this information correlates very well with different constituents of brain tissue as demonstrated in H&E stained serial sections. In contrast to previous CARS studies of brain tissue, different biological structures were visualized simultaneously and separated from each other by different colors. In the case of granule cells and Purkinje cells it was even possible to differentiate two neuronal cell types. The intense signal contrast provided by myelin represents an excellent marker for the grey matter distribution in neighboring types of tissue. At this point, we also demonstrate that the signal intensity itself is not sufficient for monitoring the white matter distribution and show how quantitative information can also be extracted from MCARS raw data. Further studies should involve the use of this effect in order to identify pathologic modifications. Based on the inspiring results retrieved from PCA processed MCARS spectra, databases could be combined with PCA and SIMCA algorithms [11,26] to provide image contrast based on the class affiliation of unknown spectra.

## Acknowledgments

We gratefully acknowledge the BMBF MEDICARS project for funding and generous support of this research-project. The excellent technical assistance of Mrs. Ginette Bortolussi is gratefully acknowledged.

#147302 - $15.00 USD Received 11 May 2011; revised 27 Jun 2011; accepted 27 Jun 2011; published 30 Jun 2011